



6-2013

Physically-Realizable Uniform Temperature Boundary Condition Specification on a Wall of an Enclosure: Part I – Problem Investigation

P. Y. C. Lee
Kutztown University of Pennsylvania

W. H. Leong
Ryerson University

Follow this and additional works at: <https://digitalcommons.pvamu.edu/aam>



Part of the [Partial Differential Equations Commons](#)

Recommended Citation

C. Lee, P. Y. and Leong, W. H. (2013). Physically-Realizable Uniform Temperature Boundary Condition Specification on a Wall of an Enclosure: Part I – Problem Investigation, *Applications and Applied Mathematics: An International Journal (AAM)*, Vol. 8, Iss. 1, Article 3.
Available at: <https://digitalcommons.pvamu.edu/aam/vol8/iss1/3>

This Article is brought to you for free and open access by Digital Commons @PVAMU. It has been accepted for inclusion in *Applications and Applied Mathematics: An International Journal (AAM)* by an authorized editor of Digital Commons @PVAMU. For more information, please contact hvkoshy@pvamu.edu.



Available at
<http://pvamu.edu/aam>
Appl. Appl. Math.
ISSN: 1932-9466

Applications and Applied
Mathematics:
An International Journal
(AAM)

Vol. 8, Issue 1 (June 2013), pp. 34 – 54

Physically-Realizable Uniform Temperature Boundary Condition Specification on a Wall of an Enclosure: Part I – Problem Investigation

P.Y.C. Lee¹ and W.H. Leong²

¹Department of Mathematics
Kutztown University of Pennsylvania
P.O. Box 730
Kutztown, Pennsylvania 19530
plee@kutztown.edu

²Department of Mechanical and Industrial Engineering
Ryerson University
350 Victoria St.
Toronto, Ontario, Canada M5B 2K3
weyleong@ryerson.ca

Received: August 21, 2012; Accepted: March 20, 2013

Abstract

Designing an experimental apparatus requires considerable amount of planning. Despite proper planning, one can easily overlook a design such as the standard uniform temperature boundary condition applied to all or portion of a wall of an experimental apparatus. Although this boundary condition is mathematically simple and precise, achieving it physically may not be that simple. This paper addresses one such three-dimensional natural convection heat transfer apparatus that was designed to measure benchmark Nusselt numbers at various Rayleigh numbers with uniform temperatures specified at two walls of the enclosure. It was found that the effect of thermal spreading/constriction resistance on one wall where this uniform temperature condition was prescribed was significant, and as a result, the uniform temperature profile based on the initial design was not physically achieved. In support of this non-uniform temperature observation, this paper presents a thermal resistance model of a plate (which is a portion of this overall heat transfer apparatus) to explain the observed temperature non-uniformity. The results obtained from the current model are validated with measured data, and in terms of a temperature difference between two locations on the plate, the approximate analytical solution is well within the experimental error of 0.03K.

Keywords: Thermal constriction/spreading resistance, uniform temperature condition, analytical solution

MSC 2010 No.: 35J25, 35M12, 35K05

1. Introduction

Heat conduction within a plate that is convectively cooled on one surface and subjected to a non-uniform heat flux over its opposite surface occurs in many engineering applications. These occur, for example, in solar collector plates, in radiative cooling of panels on satellites or space crafts, and in microelectronic circuit boards. What is important in these applications is how effectively heat travels from one part of the boundary onto another part of the boundary via heat conduction so that heat can be either used or removed.

In the microelectronics industry, for one, the effectiveness of heat dissipation from electronic components (e.g., power transistors and chips) to heat spreading plates (e.g., circuit boards and heat sinks) is very important. In analyzing the effectiveness of heat dissipation, thermal resistance is modeled, and in particular, thermal *spreading* (or *constriction*) resistance is analyzed as it may be a dominant term in the overall thermal resistance of a microelectronic board.

One of the early investigations of thermal resistance in semiconductor devices was analyzed by Kennedy (1960). Analytical solutions for axisymmetric geometry with uniform heat flux source on a finite cylinder were derived. However, because of the assumption of an isothermal condition on the heat sink side, many practical problems were not properly modeled. For thin plates and small Biot numbers, Kennedy (1960) under-predicted spreading resistances by an order of magnitude (Lee et al. (1995)).

An approximate, simple closed-form solution for calculating spreading resistances for a circular and square source placed on a rectangular plate was derived by Song et al. (1994). This approximation is based on the analytical solutions obtained by Lee et al. (1995), and the simple solution was within 10% of the analytical solution over a wide range of parameters suitable for microelectronics applications. Lee (1998) also reports that errors became large for cases where large aspect ratios for the rectangular source and plate were analyzed.

Analytical expressions for calculating spreading resistance and surface temperature field were derived by Ellison (2003) for non-circular source and spreader plate by solving a three-dimensional steady-state heat conduction equation. Dimensionless spreading resistances were presented as a function of Biot number, projected heating area, and dimensionless thickness. Yovanovich et al. (1999) and Muzychka et al. (2003) also presented three-dimensional models for analyzing thermal spreading resistances for multilayer plates and for various heat source configurations.

Instead of analyzing thermal resistance analytically, Nelson and Sayers (1992) used a control volume based finite difference method for studying spreading resistances of both axisymmetric and planar models. Bhatt and Rhee (2006) performed a systematic study on the effects of thermal spreading resistance on the overall resistance from contact to ambient for square and rectangular heat sources and spreading plates using commercial software. They found that numerical simulation can be used to perform such type of thermal analysis within 10% of exact solutions.

Thermal spreading resistances of semi-infinite media, such as a source on a half-space or a semi-infinite heat-flux tube, were also studied (for example, Mikic (1967), Cooper et al. (1969), and Yovanovich and Schneider (1977)).

The motivation behind this paper is based on analyses conducted for the design of a physically-realizable boundary condition specification on a three-dimensional experimental apparatus for natural convection studies (Leong (1996), and Leong et al. ((1998) and (1999))). In this work, a cubical enclosure was built to measure benchmark Nusselt numbers Nu for a wide range of Rayleigh numbers Ra . In measuring Nu , two different temperatures on the corresponding two opposing main walls (plates) of the enclosure were designed to be constant across each of the entire face, while the temperature on the four remaining walls (called the *sidewalls*) vary linearly between the two main walls, as depicted in Figure 1. During the initial phase of testing, temperature measurements along the sidewall in x -direction confirmed a linear temperature variation; however, the temperature at the *contact region* (see Figures 2 and 3a), where the sidewall meets the main wall, was not equal to the temperatures measured near the center of the main wall (Leong (1996)). As a result, further design changes were required to reduce the temperature non-uniformity to an acceptable level between the contact region and the entire main wall, so that a constant temperature profile can be deemed appropriate for their experimental natural convection study.

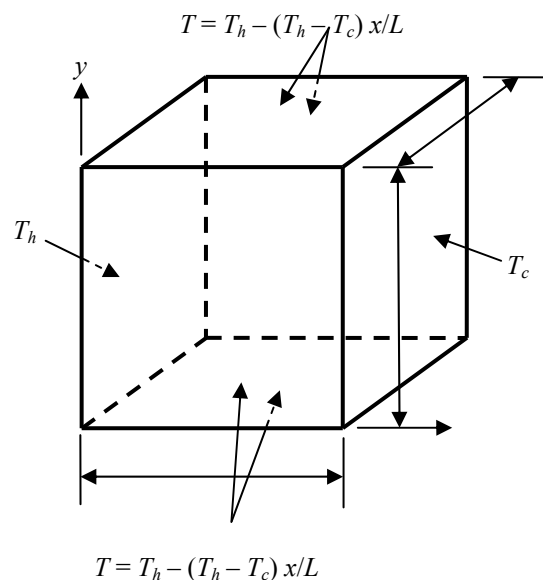


Figure 1. A sketch of cubical enclosure with its thermal boundary conditions

The physical layout of the problem analyzed in this paper is defined in Figure 2, which is based on the experimental apparatus designed by Leong (1996). A similar problem analyzed by Schneider et al. (1980) was carried out, but the current mathematical problem is a general problem based on a mixed boundary condition specification. That is, compared to the present physical problem (shown in Figure 3b), Schneider et al. (1980) assumes that the *entire* opposite boundary is in contact with an ambient fluid.

In this paper, an approximate analytical solution to a mixed boundary value problem is presented, and then this approximate solution is applied to obtain a thermal resistance model. The approximate analytical solution to the problem is verified against solutions presented by Schneider et al. (1980), and the present solution is also compared to converged finite-element solutions. Specifically, the objectives of this paper are: to fully understand the reasons for the temperature non-uniformity on the main hot plate; and to show that the approximate analytical solution presented herein supports the measured temperature difference on the main hot plate as observed by Leong (1996).

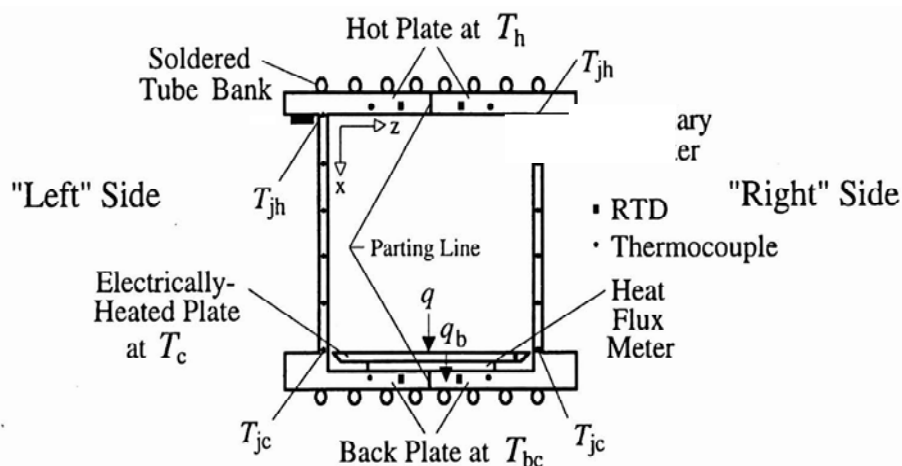


Figure 2. Original cubical experimental apparatus

2. Problem Description

Mathematical Statement of the Problem

Simplification to the problem can be achieved by considering the left-half portion of the main hot plate due to symmetry, and Figure 3 shows the geometry to be considered for analysis. In addition, groups of circulating tube banks on the top/upper portion of the plate were “lumped” into two groups of single tube bank as shown on Figure 3A.

As a result, a Cartesian coordinate system is established with the origin located at the lower left corner of the plate. The width and the thickness of the plate are denoted by b and c , respectively. The contact region where the heat flux distribution $q(x)$ is prescribed spans $2a$ at a distance e from the y -axis. Two portions of the upper surface having widths of d_1 and d_2 are in contact with fluid temperatures T_{f1} and T_{f2} , respectively, and with convective heat-transfer coefficients h_1 and h_2 , respectively. The remaining surfaces are impervious to heat transfer (that is, they are assumed adiabatic). Although in reality the bottom-interior surface of the main hot plate experiences natural convective heat flux, because the convective heat flux is so small compared to $q(x)$, it is neglected for the purpose of this study.

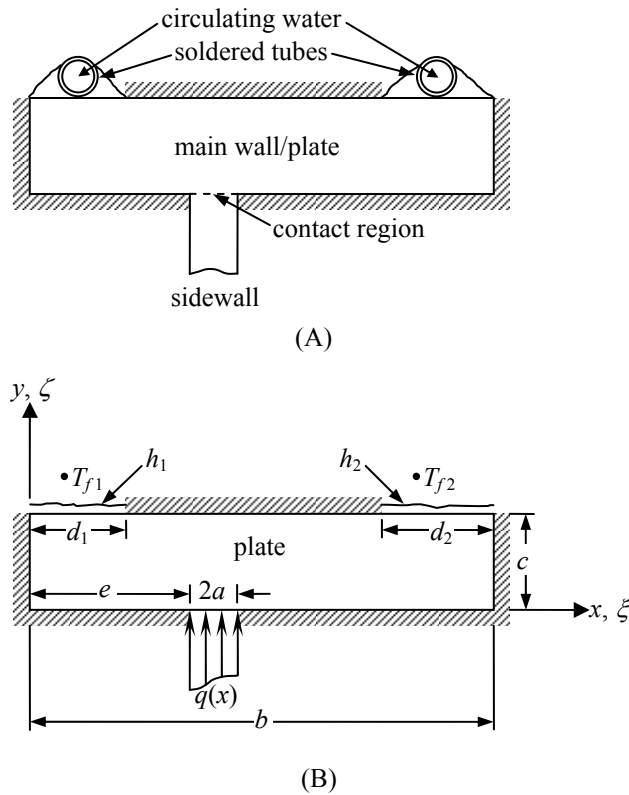


Figure 3. (A) A sketch of the physical problem, and
(B) A general representation of the Problem with defined parameters

The governing differential equation is the Laplace's equation (steady-state heat conduction in a homogeneous, isotropic conductor with thermal conductivity k and no internal heat generation):

$$\frac{\partial^2 T}{\partial x^2} + \frac{\partial^2 T}{\partial y^2} = 0, \quad (1)$$

which is subject to the boundary conditions given by:

$$x = 0, \quad 0 \leq y \leq c: \quad \frac{\partial T}{\partial x} = 0, \quad (2a)$$

$$x = b, \quad 0 \leq y \leq c: \quad \frac{\partial T}{\partial x} = 0, \quad (2b)$$

$$y = 0, \quad 0 \leq x \leq e: \quad \frac{\partial T}{\partial y} = 0, \quad e \leq x \leq e + 2a: \quad \frac{\partial T}{\partial y} = \frac{-q(x)}{k}, \quad e + 2a \leq x \leq b: \quad \frac{\partial T}{\partial y} = 0, \quad (2c)$$

$$y = c, \quad 0 \leq x \leq d_1: \frac{\partial T}{\partial y} = -\frac{1}{k} h_1 [T(x, c) - T_{f1}], \quad d_1 \leq x \leq b - d_2: \frac{\partial T}{\partial y} = 0, \\
 b - d_2 \leq x \leq b: \frac{\partial T}{\partial y} = -\frac{1}{k} h_2 [T(x, c) - T_{f2}]. \quad (2d)$$

3. Approximate Analytical Solution

In solving Equation (1), the following dimensionless variables are introduced:

$$\xi \equiv \frac{x}{b}, \quad \zeta \equiv \frac{y}{b}, \quad T^* \equiv \frac{kL(T - \overline{T_f})}{Q}, \quad (3)$$

where

$$\overline{T_f} = \frac{d_1 h_1 T_{f1} + d_2 h_2 T_{f2}}{d_1 h_1 + d_2 h_2} \quad (4)$$

is the weighted-average of the fluid temperature, and

$$Q = L \int_e^{e+2a} q(x) dx \quad (5)$$

is the total heat flow due to $q(x)$ over length L (into the page). Additional dimensionless parameters are introduced:

$$\varepsilon \equiv \frac{a}{b}, \quad \alpha \equiv \frac{c}{b}, \quad \beta_1 \equiv \frac{d_1}{b}, \quad \beta_2 \equiv \frac{d_2}{b}, \quad \eta \equiv \frac{e}{b}, \quad (6)$$

and from Equation (3), the dimensionless fluid temperatures are given by

$$T_{f1}^* = \frac{kL(T_{f1} - \overline{T_f})}{Q}, \quad T_{f2}^* = \frac{kL(T_{f2} - \overline{T_f})}{Q}, \quad (7)$$

where the average fluid temperature (Equation (4)) expressed in terms of dimensionless variables is

$$\overline{T_f} = \frac{\beta_1 Bi_1 T_{f1} + \beta_2 Bi_2 T_{f2}}{\beta_1 Bi_1 + \beta_2 Bi_2}, \quad (8)$$

and the Biot numbers/moduli are defined by

$$Bi_1 \equiv \frac{h_1 b}{k}, \quad Bi_2 \equiv \frac{h_2 b}{k}. \quad (9)$$

The main difficulty in obtaining an exact analytical temperature solution to Equation (1) based on the boundary conditions (given in Equations (2)) is due to the fact that a Robin (mixed) boundary condition (see boundary conditions along $y = c$, which is given in Equation (2d)) is imposed on one side of the plate where two subsections are in contact with the fluid (the conduction-convection condition). In Appendix A, the difficulty in obtaining an exact analytical solution is identified, and the orthogonality condition of the basis function is assumed to apply across each of these two subsections. Based on this assumption, an approximate analytical temperature solution was obtained, and is given by

$$\begin{aligned} T^*(\xi, \zeta) = T^* = & \gamma - \zeta \\ & + \sum_{n=1}^{\infty} \left\{ (\varphi_n [T_{f1}^* - (\gamma - \alpha)] - \chi_n [T_{f2}^* - (\gamma - \alpha)]) \cos(n\pi\xi) \cosh(n\pi\zeta) \right\} \\ & + \sum_{n=1}^{\infty} \left\{ \frac{2}{n\pi} \left[\frac{bL}{Q} \int_{\eta}^{\eta+2\varepsilon} q(\xi) \cos(n\pi\xi) d\xi \right] \cos(n\pi\xi) [\psi_n \cosh(n\pi\zeta) - \sinh(n\pi\zeta)] \right\} \end{aligned} \quad (10)$$

where

$$\gamma = \alpha + \frac{1}{\beta_1 Bi_1 + \beta_2 Bi_2}, \quad (11a)$$

$$\varphi_n = \frac{\frac{2}{n\pi} Bi_1 \sin(n\pi\beta_1)}{n\pi \sinh(n\pi\alpha) + (\sigma_{1,n} + \sigma_{2,n}) \cosh(n\pi\alpha)}, \quad (11b)$$

$$\chi_n = \frac{\frac{2}{n\pi} Bi_2 (-1)^{n+1} \sin(n\pi\beta_2)}{n\pi \sinh(n\pi\alpha) + (\sigma_{1,n} + \sigma_{2,n}) \cosh(n\pi\alpha)}, \quad (11c)$$

$$\psi_n = \frac{n\pi \cosh(n\pi\alpha) + (\sigma_{1,n} + \sigma_{2,n}) \sinh(n\pi\alpha)}{n\pi \sinh(n\pi\alpha) + (\sigma_{1,n} + \sigma_{2,n}) \cosh(n\pi\alpha)}, \quad (11d)$$

and

$$\sigma_{i,n} = Bi_i \left[\beta_i + \frac{1}{2n\pi} \sin(2n\pi\beta_i) \right], \quad \text{for } i = 1, 2. \quad (11e)$$

4. Thermal Resistance Model

The overall thermal resistance is defined by

$$R_o \equiv \frac{\overline{T_c} - \overline{T_f}}{Q}, \quad (12)$$

where

$$\overline{T_c} = \frac{1}{2a} \int_e^{e+2a} T(x, 0) dx, \quad (13a)$$

is the average temperature across the contact region, or in dimensionless form,

$$\overline{T_c}^* = \frac{kL(\overline{T_c} - \overline{T_f})}{Q} = \frac{1}{2\varepsilon} \int_\eta^{\eta+2\varepsilon} T^*(\xi, 0) d\xi. \quad (13b)$$

Equation (12) can be represented as dimensionless resistance defined by

$$R_o^* \equiv R_o kL = \frac{kL(\overline{T_c} - \overline{T_f})}{Q}, \quad (14)$$

which turns out to be simply the average dimensionless temperature over the contact region (Equation (13b)):

$$R_o^* = \overline{T_c}^* = \frac{1}{2\varepsilon} \int_\eta^{\eta+2\varepsilon} T^*(\xi, 0) d\xi. \quad (15)$$

Substituting the dimensionless temperature solution, Equation (10), into Equation (15), the overall thermal resistance is

$$R_o^* = \gamma + \sum_{n=1}^{\infty} \left\{ \frac{1}{n\pi\varepsilon} [\varphi_n (T_{f1}^* - \gamma) - \chi_n (T_{f2}^* - \gamma)] \cos(n\pi(\eta + \varepsilon)) \sin(n\pi\varepsilon) \right\} \\ + \sum_{n=1}^{\infty} \left\{ \frac{2}{n^2 \pi^2 \varepsilon} \left[\frac{bL}{Q} \int_\eta^{\eta+2\varepsilon} q(\xi) \cos(n\pi\xi) d\xi \right] \psi_n \cos(n\pi(\eta + \varepsilon)) \sin(n\pi\varepsilon) \right\}, \quad (16)$$

where γ , φ_n , χ_n , and ψ_n are defined in Equation (11). The dimensionless overall thermal resistance has the same dependent variables as the dimensionless temperature field, except that it is independent of the two spatial coordinates ξ and ζ .

In Equation (16), the first term γ is comprised of resistances due to conduction across the plate thickness c , R_{cond}^* ($=\alpha$), and due to convection at the solid-fluid interfaces, R_{conv}^* ($=1/(\beta_1 Bi_1 + \beta_2 Bi_2)$), (Equation (11a)). The second and third terms are resistances due to thermal spreading/constriction $R_{s/c}^*$ which is given by

$$R_{s/c}^* = \sum_{n=1}^{\infty} \left\{ \frac{1}{n\pi\varepsilon} [\varphi_n (T_{f1}^* - (\gamma - \alpha)) - \chi_n (T_{f2}^* - (\gamma - \alpha))] \cos(n\pi(\eta + \varepsilon)) \sin(n\pi\varepsilon) \right\} + \sum_{n=1}^{\infty} \left\{ \frac{2}{n^2\pi^2\varepsilon} \left[\frac{bL}{Q} \int_{\eta}^{\eta+2\varepsilon} q(\xi) \cos(n\pi\xi) d\xi \right] \psi_n \cos(n\pi(\eta + \varepsilon)) \sin(n\pi\varepsilon) \right\}. \tag{17}$$

Furthermore, Equation (17) is comprised of two terms; the first term is resistance due to spreading/constriction of heat flow at the solid-fluid interfaces; and the second term is the effect of spreading as heat is dispersed from the contact region to the remaining sections of the plate.

5. Special Cases for the Heat Flux Profiles

In this section, three different heat flux distributions will be used to quantify thermal spreading resistance. As suggested by Schneider et al. (1980), the heat flux profiles to be considered are given by

$$q(x) = q_0(1 - u^2)^m, \quad m = -1/2, 0, 1/2, \tag{18}$$

where q_0 is a constant heat flux/parameter, and u is the local co-ordinate system where the heat flux distribution is prescribed. That is,

$$u \equiv \frac{1}{a}(x - e) - 1 = \frac{1}{\varepsilon}(\xi - \eta) - 1. \tag{19}$$

These heat flux distributions, given in Equation (18), are shown graphically in Figure 4.

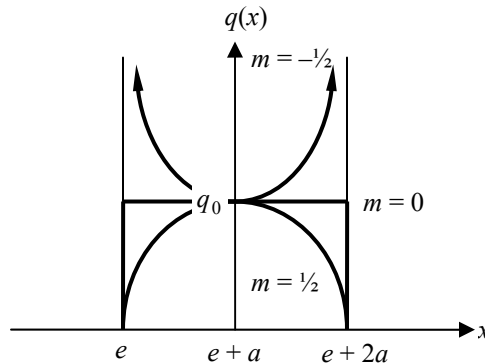


Figure 4. Three Cases of Heat Flux Distribution

For convenience, we define $F_n(\eta, \varepsilon)$ by:

$$F_n(\eta, \varepsilon) \equiv \frac{bL}{Q} \int_{\eta}^{\eta+2\varepsilon} q(\xi) \cos(n\pi\xi) d\xi. \tag{20}$$

Based on the heat flux profiles of Equation (18), Table 1 lists the functional forms of Equation (20), for $m = -1/2, 0,$ and $1/2$ in terms of trigonometric and Bessel functions, $J_0(\cdot)$ and $J_1(\cdot)$ (Gradshteyn and Ryzhik (1965)).

Table 1. Functional forms of $F_n(\eta, \varepsilon)$ based on the choice of m

m	$F_n(\eta, \varepsilon)$	$F_n(\varepsilon)$, for $\eta = -\varepsilon$
-1/2	$J_0(n\pi\varepsilon) \cos(n\pi(\eta + \varepsilon))$	$J_0(n\pi\varepsilon)$
0	$\sin(n\pi\varepsilon) \cos(n\pi(\eta + \varepsilon))/n\pi\varepsilon$	$\sin(n\pi\varepsilon)/n\pi\varepsilon$
1/2	$2 J_1(n\pi\varepsilon) \cos(n\pi(\eta + \varepsilon))/n\pi\varepsilon$	$2 J_1(n\pi\varepsilon)/n\pi\varepsilon$

6. Results and Discussion

Verification of the Present Solution

To assess whether the approximate analytical solutions represented by Equations (10), (16), and (17) agree well with existing solutions, a set of problem presented by Schneider et al. (1980) is considered. The problem definition to be analyzed is shown in Figure 5 below.

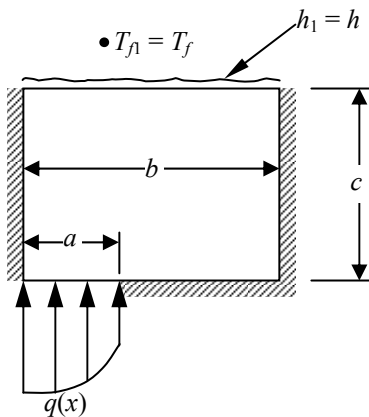


Figure 5. Problem Analyzed by Schneider et al. (1980)

Based on Figure 5 the following parameters introduced in this paper are matched to those parameters considered by Schneider et al. (1980):

- a) $\beta_1 = \beta = 1, \beta_2 = 0$ (i.e., $d_1 = b, d_2 = 0$);
- b) $Bi_1 = Bi$ (i.e., $h_1 = h$);
- c) $T_{f1}^* = 0$ (i.e., $T_{f1} = T_f = \overline{T_f}$),
- d) $\eta = -\varepsilon$ (i.e., half of the heat flux distribution).

Under these specifications, it can be shown that, from Equation (11b) and (11c), $\varphi_n = 0$ and $\chi_n = 0$, respectively. The dimensionless temperature distribution T^* , the dimensionless overall thermal

resistance R_o^* , and the dimensionless thermal spreading/constriction resistance $R_{s/c}^*$ reduce to the exact analytical solutions to this boundary value problem, and all coincide with the analytical solutions provided by Schneider et al. (1980). The corresponding exact analytical solutions are given by

$$T^* = \gamma - \zeta + \sum_{n=1}^{\infty} \left\{ \frac{2}{n\pi} \cdot F_n(\varepsilon) \cdot \cos(n\pi\xi) [\psi_n \cosh(n\pi\zeta) - \sinh(n\pi\zeta)] \right\}, \quad (21)$$

$$R_o^* = \gamma + \sum_{n=1}^{\infty} \frac{2}{n^2 \pi^2 \varepsilon} \cdot F_n(\varepsilon) \cdot \psi_n \sin(n\pi\varepsilon), \quad (22)$$

and

$$R_{s/c}^* = \sum_{n=1}^{\infty} \frac{2}{n^2 \pi^2 \varepsilon} \cdot F_n(\varepsilon) \cdot \psi_n \sin(n\pi\varepsilon), \quad (23)$$

respectively, where

$$\gamma = \alpha + \frac{1}{Bi}, \quad (24a)$$

$$\psi_n = \frac{n\pi \cosh(n\pi\alpha) + Bi \sinh(n\pi\alpha)}{n\pi \sinh(n\pi\alpha) + Bi \cosh(n\pi\alpha)}, \quad (24b)$$

and the functional forms of $F_n(\varepsilon)$ are also listed in Table 1.

The effect of thermal spreading/constriction resistance for this problem is discussed in detail by Schneider et al. (1980). In summary, they found that the thermal constriction resistance is relatively insensitive to the applied heat flux profile. They also found that the maximum thermal constriction resistance is obtained for the combination where both Bi and α are small; conversely, the minimum thermal constriction resistance is obtained for the combination where Bi is large and α is small. Their study was based on the following ranges of parameters: $0.01 \leq Bi \leq 100$, $0.05 \leq \alpha \leq 2.0$, and $0.01 \leq \varepsilon \leq 1.0$.

7. Verification of the Present Approximate Analytical Solution

Based on the problem definition of Figure 3b, the physical dimensions are obtained from Leong (1996): $2a = 3.2$ mm, $b = 78$ mm, $c = 9.53$ mm, $d_1 = d_2 = d = 22$ mm, and $e = 11$ mm. As a result, $\alpha = 0.122$, $\beta_1 = \beta_2 = \beta = 0.282$, $\eta = 0.141$, and $\varepsilon = 0.0205$. Tests of the experimental apparatus were conducted at a fixed circulating water flow rate of 1.17 litres/min in each tube at the upper two portions of the plate, so it is assumed that $T_{f1} = T_{f2} = T_f = \overline{T_f}$ (that is, $T_{f1}^* = T_{f2}^* = 0$) and that $Bi_1 = Bi_2 = Bi$ (since $h_1 = h_2 = h$). The plate is made out of copper with a thermal conductivity value of $k = 388$ W/(mK).

Under these specifications, the approximate analytical solutions to Equations (10), (16), and (17) are given by

$$T^* = \gamma - \zeta + 2(\gamma - \alpha) \sum_{n=2,4,6\dots}^{\infty} \chi_n \cos(n\pi\xi) \cosh(n\pi\zeta) + 2 \sum_{n=1}^{\infty} \frac{1}{n\pi} \cdot F_n(\eta, \varepsilon) \cdot \cos(n\pi\xi) [\psi_n \cosh(n\pi\zeta) - \sinh(n\pi\zeta)], \quad (25)$$

$$R_o^* = \gamma + 2(\gamma - \alpha) \sum_{n=2,4,6\dots}^{\infty} \frac{1}{n\pi\varepsilon} \chi_n \cos(n\pi(\eta + \varepsilon)) \sin(n\pi\varepsilon) + 2 \sum_{n=1}^{\infty} \frac{1}{n^2 \pi^2 \varepsilon} \cdot F_n(\eta, \varepsilon) \cdot \psi_n \cos(n\pi(\eta + \varepsilon)) \sin(n\pi\varepsilon), \quad (26)$$

and

$$R_{s/c}^* = 2(\gamma - \alpha) \sum_{n=2,4,6\dots}^{\infty} \frac{1}{n\pi\varepsilon} \chi_n \cos(n\pi(\eta + \varepsilon)) \sin(n\pi\varepsilon) + 2 \sum_{n=1}^{\infty} \frac{1}{n^2 \pi^2 \varepsilon} \cdot F_n(\eta, \varepsilon) \cdot \psi_n \cos(n\pi(\eta + \varepsilon)) \sin(n\pi\varepsilon), \quad (27)$$

respectively, where

$$\gamma = \alpha + \frac{1}{2Bi\beta}, \quad (28a)$$

$$\varphi_n = \frac{\frac{2}{n\pi} Bi \sin(n\pi\beta)}{n\pi \sinh(n\pi\alpha) + 2\sigma_n \cosh(n\pi\alpha)}, \quad (28b)$$

$$\chi_n = \begin{cases} \varphi_n, & \text{for } n = 1, 3, 5, \dots \\ -\varphi_n, & \text{for } n = 2, 4, 6, \dots \end{cases}, \quad (28c)$$

$$\psi_n = \frac{n\pi \cosh(n\pi\alpha) + 2\sigma_n \sinh(n\pi\alpha)}{n\pi \sinh(n\pi\alpha) + 2\sigma_n \cosh(n\pi\alpha)}, \quad (28d)$$

and, from Equation (11e),

$$\sigma_n = \sigma_{1,n} = \sigma_{2,n} = Bi \left[\beta + \frac{1}{2n\pi} \sin(2n\pi\beta) \right]. \quad (28e)$$

What remains unanswered thus far is which shape of the heat flux distribution along the contact region is adequate before comparing the approximate analytical solution to the measured data.

Based on the following two observations and findings, a uniform heat flux profile, i.e. $m = 0$, can be assumed along the contact region:

1. Although the three heat flux distributions are distinctly different, thermal spreading resistances do not depend strongly on the shape of the heat flux profiles over a wide range of Bi values as shown in Figure 6. (This was also reported by Schneider et al. (1980).) If the actual heat flux distribution falls within the extreme cases of $m = -1/2$ and $m = 1/2$, the uniform heat flux profile will provide a good approximation.
2. Along the sidewall, the Biot number $Bi_t \equiv h_{nc}t/k$ can be determined to justify the nature of the heat flux profile. These values were used to calculate Bi_t : $h_{nc} = 25 \text{ W}/(\text{m}^2\text{K})$ for high gaseous natural convection heat transfer, $t = 2a = 3.2 \text{ mm}$, and $k = 388 \text{ W}/(\text{mK})$, which gives $Bi_t = 0.0002 \ll 0.1$. Since this value is small, the temperature gradient across the thickness of the sidewall is negligible, and thus the assumption of uniform heat flux profile along the sidewall is valid.

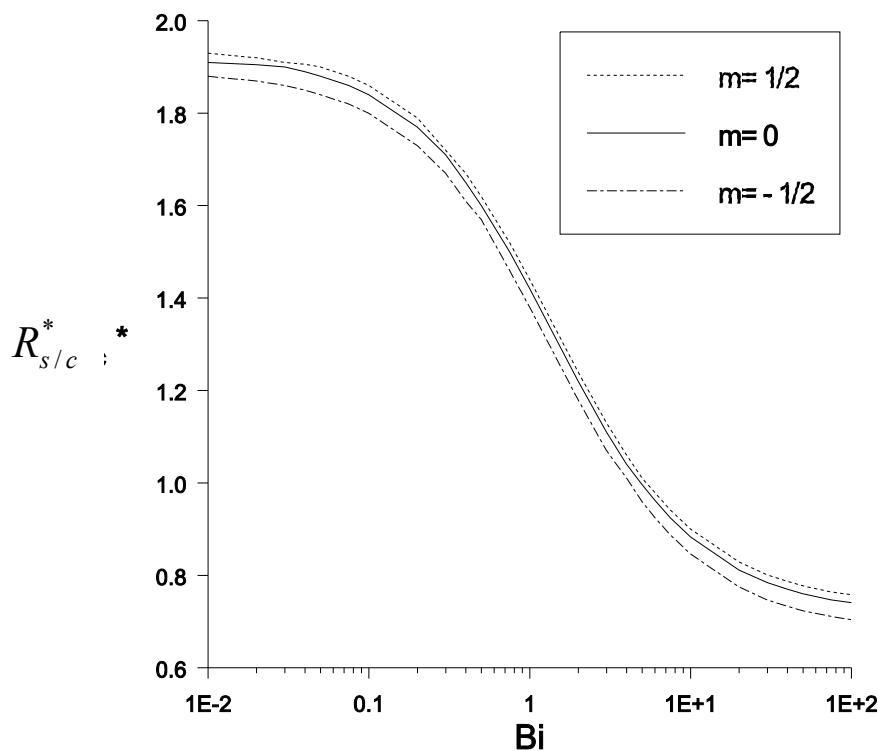


Figure 6. Thermal spreading/constriction resistance based on the actual configuration (Leong (1996)) for three different heat flux profiles ($m = -1/2, 0, 1/2$).

From Equations (26), (27) and (28a), the effects of Bi on thermal resistances due to conduction R_{cond}^* , convection R_{conv}^* , spreading/constriction $R_{s/c}^*$, and overall R_o^* are calculated, and are plotted in Figure 7. It is clear that the overall thermal resistance possesses two asymptotes: as $Bi \rightarrow 0$, R_o^* approaches R_{conv}^* ($= 1/(2Bi\beta)$); and for $Bi \gg 1$, R_o^* approaches $R_{s/c}^*$. It is also apparent from Figure 7 that in order to reduce the thermal spreading/constriction resistance, it is suitable to increase Bi to values greater than 1, but the effect is relatively weak.

In studying the effects of thermal spreading/constriction resistance from an experimental point of view, four cases were considered. In each case, different sets of the main wall (plate) temperatures, T_h and T_c , were prescribed (Leong (1996)). As a result, each of the four cases has a slightly different Bi value. In each case, a series of temperature differences, δT 's, was measured between $\zeta_1 = 0.162$ ($x_1 = 12.6$ mm) and $\zeta_2 = 0.75$ ($x_2 = 58.5$ mm) along $\zeta = 0$ ($y = 0$), using a thermopile embedded in the plate. Then, a mean value, $\overline{\delta T}$, of these temperature differences was obtained by averaging over 120 (δT) measurements. Also, the uniform heat flux, q_0 , for each case was determined using Fourier's law based on the temperature gradient measurements along the sidewall. According to Leong (1996), the mean values of measured temperature differences are considered to have negligible precision error, but with a bias error of ± 0.03 K.

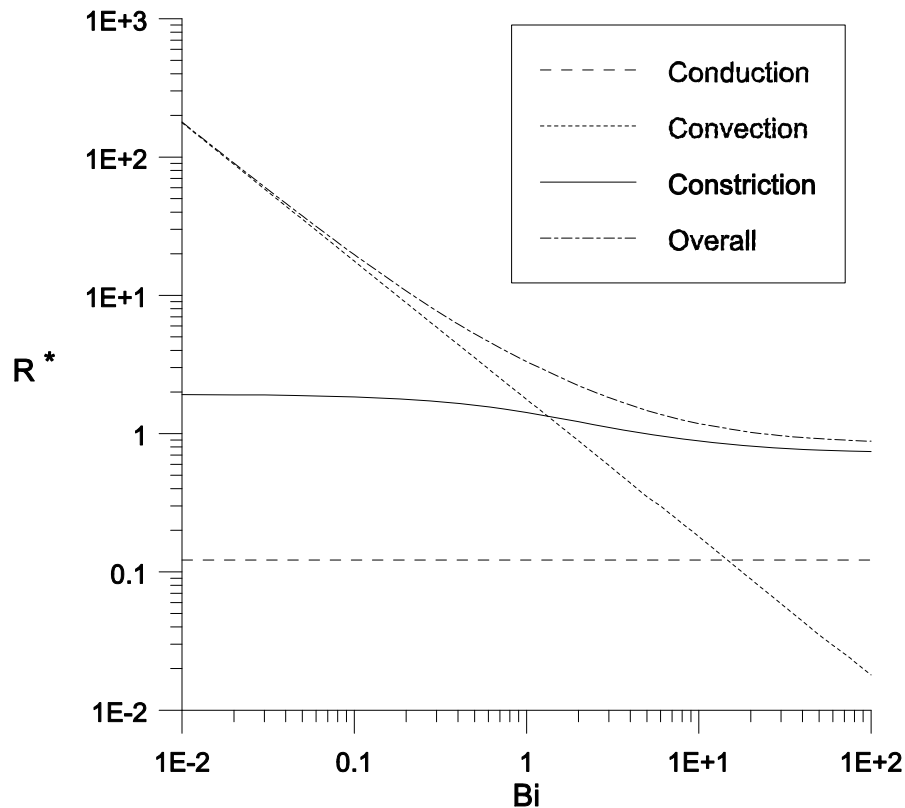


Figure 7. Contribution of Thermal Resistances Due to Conduction, Convection and Spreading/Constriction

A comparison of the approximate analytical temperature solution, Equation (25), with the finite-element method (FEM) temperature solution based on the “fine” grid (see Appendix B) shows that (for the practical range of interest $1.2 \leq Bi \leq 5$ and $0 \leq -q_0 \leq 200$ kW/m²), Equation (25) is found to be less than 0.7% of the FEM based “fine” grid numerical solution. For this reason, the present approximate analytical solution, Equation (25), was used in analysing the temperature non-uniformity along the bottom plate, and used in analysing the thermal resistance of the plate. To validate the present approximate analytical solution, measured q_0 and Bi values are used as inputs to obtain the temperature difference, δT , derived from the approximate solution, Equation (25):

$$\delta T = T(x_2, 0) - T(x_1, 0) = \frac{2aq_0}{k} \delta T^* , \tag{29}$$

where

$$\begin{aligned} \delta T^* &= T^*(\xi_2, 0) - T^*(\xi_1, 0) \\ &= 2(\gamma - \alpha) \sum_{n=2,4,6\dots}^{\infty} \chi_n [\cos(n\pi\xi_2) - \cos(n\pi\xi_1)] \\ &\quad + \sum_{n=1}^{\infty} \frac{2}{n\pi} \cdot F_n(\eta, \varepsilon) \cdot \psi_n [\cos(n\pi\xi_2) - \cos(n\pi\xi_1)] \end{aligned} \tag{30}$$

Table 2. Comparison of results between measured and present model

Case	ΔT^+ (K)	q_0^+ (W/m ²)	Bi^+	$\delta \bar{T}^+$ (K)	δT^{++} (K)	$\delta T^{++} - \delta \bar{T}^+$ (K)	$(\delta \bar{T} / \Delta T)^+$
1	4.08	-11000	1.373	0.164	0.179	0.015	4.02%
2	11.9	-32100	1.484	0.521	0.512	-0.009	4.38%
3	21.2	-57500	1.695	0.869	0.884	0.015	4.10%
4	31.2	-84800	1.703	1.292	1.302	0.010	4.14%

⁺ Experimental (Leong(1996)); ⁺⁺ Present Model

For comparison, Table 2 lists the measured temperature differences, $\delta \bar{T}$, and the temperature differences based on the present model, δT , Equation (29). Among the four cases measured, the largest difference between the measured data and the results based on the present model is 0.015 K, and are in excellent agreement with the experimental data. Also, shown in the table, the approximate analytical results are well within the experimental uncertainty of 0.03 K.

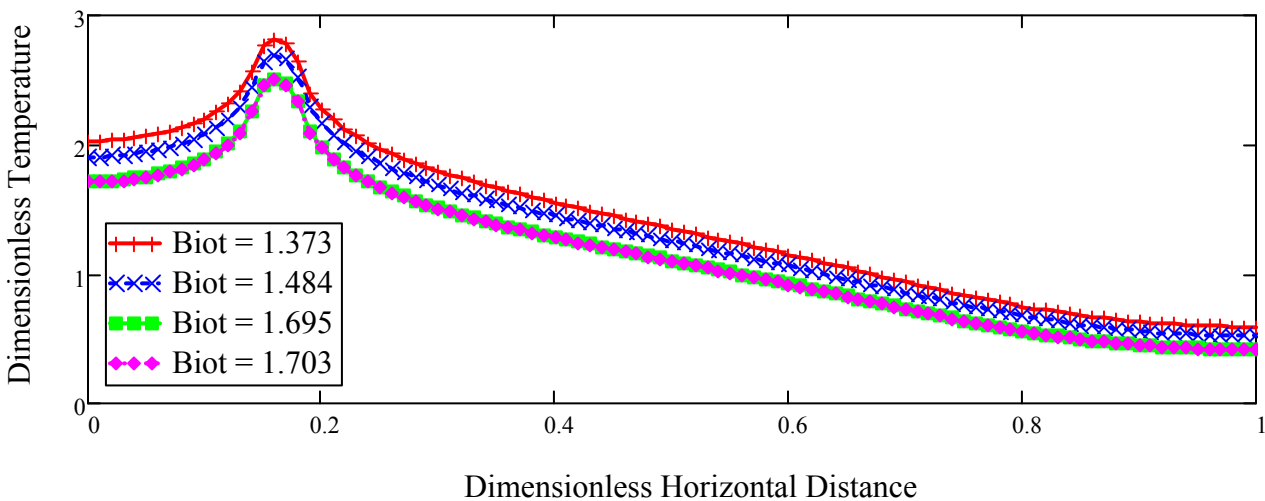


Figure 8. Dimensionless temperature profile $T^*(\xi, 0)$ versus dimensionless horizontal distance ξ

Moreover, Table 2 lists the measured Bi 's for this problem, and they fall within the range ($1 \leq Bi \leq 2$) where the effect of thermal spreading/constriction resistance is important. As shown in Figure 7, the effect of spreading/constriction resistance is approximately 46% of the overall thermal resistance.

To illustrate the effect of thermal spreading/constriction resistance on the plate on the temperature field, the dimensionless temperature profiles along the bottom boundary of the plate ($y = 0$ or $\zeta = 0$) are shown in Figure 8 for the four experimental cases (corresponding to the four Bi number cases). These temperature profiles show dramatic temperature non-uniformity near the contact and surrounding regions of the plate.

Although the measured temperature difference, $\overline{\delta T}$, was about 4% of the overall temperature difference of the enclosure, $\Delta T (= T_h - T_c)$, the design was considered to be a failure as compared to the main objective of $|\overline{\delta T} / \Delta T| \leq 1\%$ for the benchmark experimental study. This meant that a redesign of the apparatus had to be made in order to meet the main objective of the study. A second part of this paper (Lee and Leong (2012)) presents a methodology to reduce the temperature non-uniformity from about 4% to less than 1% error.

8. Concluding Remarks

Thermal spreading/constriction resistance in a plate with a non-uniform heat flux region on one surface and two convectively cooled subsections on the opposite surface has been analytically investigated. For this general mixed boundary value problem, an approximate analytical solution is obtained for temperature, overall thermal resistance, and thermal spreading/constriction resistance. In fact, the present solution is exact with an existing solution in literature. A comparison between the approximate analytical temperature solutions with the numerical finite-element temperature solutions shows that for the geometry of the plate and for the practical range of interest $1.2 \leq Bi \leq 5$ and $0 \leq -q_o \leq 200 \text{ kW/m}^2$, the approximate analytical solution is less than 0.7% of the "fine" finite-element numerical grid based solution.

As part of one of two main objectives of this paper, it was determined that thermal spreading/constriction resistance strongly affects the temperature distribution surrounding the contact region for Bi values greater than one. From the four experimental cases, measured temperature differences between the contact region and a location on the plate away from the contact region show obvious temperature non-uniformity in the plate. The present analytical model is in excellent agreement with measured data, and is well within the uncertainty of the measurements.

Due to the general form of the present model, it can be adapted to analyzing a number of similar engineering applications. The approximate analytical solution can serve to verify any computer codes dealing with heat conduction simulation.

Acknowledgement

Financial support provided by the Natural Sciences and Engineering Research Council of Canada for this work is greatly appreciated. Also, financial support from the Professional Development Fund, the Department of Mathematics, and the College of Liberal Arts and Science of Kutztown University is also acknowledged with gratitude.

Nomenclature

a	= half-width of contact at sidewall, m
b	= width of plate, m
Bi	= Biot number/modulus, hb/k , or R_{cond}/R_{conv}
c	= plate thickness, m
d	= fluid contact width, m
e	= location of sidewall heat flux region, m
$F_n(\eta, \varepsilon)$	= functional form for sidewall heat flux profile
h	= heat transfer coefficient, $W/(m^2K)$
k	= thermal conductivity, $W/(mK)$
L	= length of plate into the page, m
m	= shape parameter for heat flux profile, $q(x)$
Q	= total heat flow at sidewall, Equation (5), W
$q(x)$	= heat flux profile of the sidewall, W/m^2
R	= thermal resistance, K/W
R_o	= overall/total thermal resistance, K/W
$R_{s/c}$	= thermal spreading/constriction resistance, K/W
T	= temperature, K
\bar{T}	= mean temperature, K
u	= local co-ordinates
x, y	= Cartesian co-ordinate
α	= dimensionless thickness, c/b
β	= dimensionless fluid contact width, d/b
$\chi_n, \varphi_n, \psi_n$	= function/parameter
δT	= temperature difference, $T(\xi_2, 0) - T(\xi_1, 0)$, K
ε	= dimensionless half contact length, a/b
γ	= dimensionless conduction and convection resistances
η	= dimensionless distance to sidewall location, e/b
$\sigma_n, \sigma_{i,n}$	= function/parameter
ξ, ζ	= dimensionless co-ordinate, x/b and y/b
<i>Superscripts</i>	
*	= dimensionless variable
<i>Subscripts</i>	
1, 2	= subsection of circulating fluid
f	= fluid
o	= sidewall (or contact), overall/total, or otherwise noted

REFERENCES

- Bhatt, A. and Rhee, J. (2006). Thermal Spreading Resistance for Square and Rectangular Entities, Proc. of 11th Int. Symposium on Advanced Packaging Materials: Processes, Properties and Interfaces, Atlanta, GA, pp. 175-178.
- Cooper, M.G., Mikic, B.B. and Yovanovich, M. M. (1969). Thermal Contact Conductance, Int. J. Heat Mass Transfer, **12**, pp. 279-300.
- Ellison, G.N. (2003). Maximum Thermal Spreading Resistance for Rectangular Sources and Plates with Nonunity Aspect Ratios, IEEE Trans. Component and Packaging Technologies, **26** (2), pp. 439-454.
- Gradshteyn, I.S. and Ryzhik, I.M. (1965). *Tables of Integrals, Series, and Products*, 4th Ed., Academic Press, New York.
- Kennedy, D.P. (1960). Spreading Resistance in Cylindrical Semiconductor Devices, J. Applied Physics, **31**, pp. 1490-1497.
- Klein, S.A., Beckman, W.A., and Myers, G.E. (2001). FEHT Finite Element Analysis, Version 7.155, Wiley, F-Chart Software.
- Lee, P.Y.C. and Leong, W.H. (2013). Physically-Realizable Uniform Temperature Boundary Condition Specification on a Wall of an Enclosure: Part II – Problem Solution, International Journal of Applications and Applied Mathematics (AAM).
- Lee, S. (1998). Calculating Spreading Resistance in Heat Sinks, Electronics Cooling Magazine, **4** (1).
- Lee, S., Song, S., Au V. and Moran, K.P. (1995). Constriction/Spreading Resistance Model for Electronics Packaging, Proc. of 4th ASME/JSME Thermal Engineering Joint Conf., **4**, Maui, HI, pp. 199-206.
- Leong, W.H. (1996). Benchmark Experiments on Natural Convection Heat Transfer Across a Cubical Cavity, Ph.D. Thesis, Department of Mechanical Engineering, University of Waterloo, Waterloo, Ontario, Canada.
- Leong, W.H., Hollands, K.G.T., and Brunger, A.P. (1998). On a Physically-Realizable Benchmark Problem in Internal Natural Convection, Int. J. Heat Mass Transfer, **41** (23), pp. 3817-3828.
- Leong, W.H., Hollands, K.G.T., and Brunger, A.P. (1999). Experimental Nusselt Numbers for a Cubical-Cavity Benchmark Problem in Natural Convection, Int. J. Heat Mass Transfer, **42** (11), pp. 1979-1989.
- Mikic, B.B. (1967). Thermal Contact Resistance”, Sc.D. Thesis, Department of Mechanical Engineering, MIT, Cambridge, Massachusetts.
- Muzychka, Y.S., Culham, J.R., and Yovanovich, M.M. (2003). Thermal Spreading Resistance of Eccentric Heat Sources on Rectangular Flux Channels, ASME J. Electronic Packaging, **1** (2), pp. 178-185.
- Nelson, D.J. and Sayers, W.J. (1992). A Comparison of 2-D Planar, Axisymmetric and 3-D Spreading Resistances”, Proc. of 8th Annual IEEE Semiconductor Thermal Measurement and Management Symposium, Austin, TX, pp. 62-68.
- Schneider, G.E., Yovanovich, M.M. and Cane, R.L.D. (1980). Thermal Resistance of a Convectively Cooled Plate with Nonuniform Applied Flux, J. Spacecraft Rockets, AIAA 78-86R, **17** (4), pp. 372-376.

- Song, S., Lee, S. and Au, V. (1994). Closed Form Equation for Thermal Constriction/Spreading Resistances with Variable Resistance Boundary Condition, Proc. of the 1994 IEPS Conf., pp. 111-121.
- Yovanovich, M.M. and Schneider, G.E. (1977). Thermal Constriction Resistance Due to a Circular Annular Contact, AIAA Progress in Astronautics and Aeronautics, Thermophysics of Spacecraft and Outer Planet Entry Probes, **56**, edited by A.M. Smith, New York, pp. 141-154.
- Yovanovich, M.M., Muzychka, Y.S. and Culham, J.R. (1999). Spreading Resistance of Isoflux Rectangles and Strips on Compound Flux Channels, J. Thermophysics and Heat Transfer, **13** (4), pp. 495-500.

Appendix A

The main difficulty in solving this boundary value problem analytically is due to the mixed boundary condition along the portion of the boundary along $y = c$, where the solid is in contact with the fluid (as defined in the boundary condition given in Equation (2d)).

In the derivation of the solution via the method of separation of variables, the solution methodology hinges on the key idea that the orthogonality condition applies along the two subsections where the fluid is in contact with the solid. That is, after applying the mixed boundary condition at $y = c$, given by Equation (2d), the form of the Fourier series solution is set up to as follows:

$$\left. \frac{\partial T}{\partial y} \right|_{y=c} = \sum_{n=0}^{\infty} [\lambda_n f(\lambda_n c)] \cos(\lambda_n x) = \begin{cases} -\frac{h_1}{k} (T(x, c) - T_{f1}), & 0 \leq x \leq d_1 \\ 0, & d_1 \leq x \leq b - d_2 \\ -\frac{h_2}{k} (T(x, c) - T_{f2}), & b - d_2 \leq x \leq b \end{cases} \quad (\text{A.1})$$

where $f(\lambda_n c)$ is a function involving all Fourier expansion coefficients introduced in the problem, and $T(x, c)$ is given by:

$$T(x, c) = \sum_{n=0}^{\infty} [f(\lambda_n c)] \cos(\lambda_n x). \quad (\text{A.2})$$

One approach for obtaining the Fourier expansion coefficients is to substitute Equation (A.2) into the piece-wise boundary condition, Equation (A.1), multiply both sides by $\cos(\lambda_n x)$, and then integrate both sides with respect to x from $x = 0$ to b . As a result, this is given by:

$$\int_0^b \left(\sum_{n=0}^{\infty} [\lambda_n f(\lambda_n c)] \cos(\lambda_n x) \cos(\lambda_m x) \right) dx = \int_0^b \left(-\frac{h_1}{k} \left(\left\{ \sum_{n=0}^{\infty} [f(\lambda_n c)] \cos(\lambda_n x) \right\} - T_{f1} \right) - \frac{h_2}{k} \left(\left\{ \sum_{n=0}^{\infty} [f(\lambda_n c)] \cos(\lambda_n x) \right\} - T_{f2} \right) \right) \cos(\lambda_m x) dx. \quad (\text{A.3})$$

Using the orthogonality condition for $n \neq m$, the left-hand side of Equation (A.3) simplifies to

$$\int_0^b \lambda_m f(\lambda_m c) \cos^2(\lambda_m x) dx, \quad (\text{A.4})$$

for $n = m$, which can be easily integrated. But the right-hand side of Equation (A.3) does not simplify since orthogonality in each of the two terms involving definite integrals along the two sub-sections given by

$$-\frac{h_1}{k} \int_0^{d_1} \left(\sum_{n=0}^{\infty} [f(\lambda_n c)] \cos(\lambda_n x) \cos(\lambda_m x) \right) dx - \frac{h_2}{k} \int_{b-d_2}^b \left(\sum_{n=0}^{\infty} [f(\lambda_n c)] \cos(\lambda_n x) \cos(\lambda_m x) \right) dx \quad (\text{A.5})$$

does not apply. That is, across these two sub-intervals, the Fourier series may still remain as an infinite series.

Instead, a solution consistent with the Fourier series expansion solution is sought, and it is assumed here that the orthogonality condition *exists along these two sub-intervals*. That is, the two definite integrals in Equation (A.5) are *assumed zero* for $n \neq m$. This way, all Fourier coefficients introduced are aligned, and are obtained by systematically applying the boundary conditions.

In APPENDIX B, a comparison of the approximate analytical temperature solution based on this orthogonality assumption with a grid-independent/converged Finite-Element Method (FEM) numerical solution is presented.

APPENDIX B

To demonstrate the accuracy of the orthogonality assumption/simplification along the two sub-sections on the temperature field, a comparison of the approximate analytical temperature solution based on this assumption with the finite-element method (FEM) temperature solution is presented for the practical range of interest given by $1.2 \leq Bi \leq 5$ and $0 \leq -q_o \leq 200 \text{ kW/m}^2$. A standard FEM software was used (Klein et al. (2001)), and for all comparisons presented, a uniform (constant) heat flux profile was assumed across the contact region. Before the comparative study was conducted, nine nodal temperatures were identified so that temperature comparisons can be made. See Figure B.1 below.

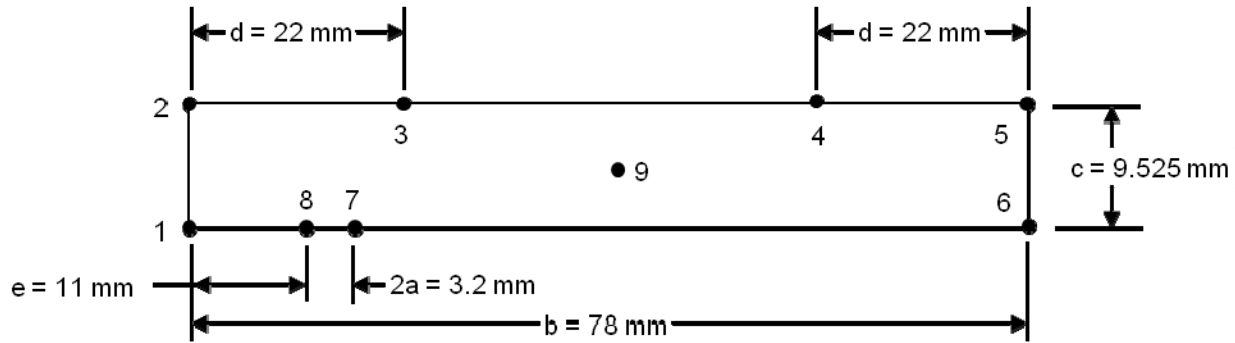


Figure B.1: Geometry of the Problem with Identified Nodes for Temperature Solution Comparisons.

Also, in selecting a grid independent temperature for this comparative study, two different grids were chosen, where the total number of nodes used in the study were 263 nodes (“coarse”) and 965 (“fine”). As the total number of grids increased from “coarse” to “fine”, the temperature values at these nine nodes were all less than 0.07% of the “fine” grid temperature values for the practical range of interest $1.2 \leq Bi \leq 5$ and $0 \leq -q_o \leq 200 \text{ kW/m}^2$ (not shown here). A third chosen “finer” grid was planned but was not chosen in this study because all FEM solutions based on these two grids were within less than 0.07% of the “fine” solution. This “fine” grid was then used in the comparison of the approximate analytical temperature solution with the FEM based temperature solution.

Presented in Table B.1 are the maximum temperature difference based on the fine FEM and the approximate analytical temperature solutions from each of the nine nodes. In all of the cases studied, $-q_o = 200 \text{ kW/m}^2$ was considered, which is the highest heat flux considered¹. In all cases considered, the maximum differences for all the cases studied occurred in Node 3. As shown in the table below, the approximate analytical temperature solutions for various Bi cases considered at each of the nine nodes are in excellent agreement (less than 0.7%) with the corresponding “fine” grid FEM numerical temperature solutions; for $-q_o < 200 \text{ kW/m}^2$, the differences will be lower than 0.7%.

Table B.1. Comparison of temperatures at node 3 between numerical and analytical solutions

Bi	Numerical Temperature Solution (°C)	Approximate Analytical Temperature Solution (°C)	Difference (%)
1.2	16.67	16.78	-0.66
1.3	16.89	17.00	-0.65
1.4	17.08	17.19	-0.64
1.5	17.24	17.35	-0.64
2.0	17.83	17.94	-0.62
3.0	18.45	18.57	-0.65
4.0	18.78	18.90	-0.64
5.0	18.98	19.10	-0.63

¹ The maximum value of $-q_o = 200 \text{ kW/m}^2$ was chosen to reflect a severe physical case. To physically achieve this, a temperature difference between the hot and cold plates needs to be approximately $65 \text{ }^\circ\text{C}$, which is very high. Although in the validation exercise the highest temperature difference presented is $31.2 \text{ }^\circ\text{C}$ (see Table 2), all of the experimental temperature difference cases considered by Leong (1996) were within $15 \text{ }^\circ\text{C}$. The main reason for this was to ensure that the condition to the Boussinesq approximation is valid so that computational fluid dynamics (CFD) solutions can also be simulated and compared to the experimental results.